



Cite this: *Nanoscale*, 2019, **11**, 8864

Thulium doped LaF₃ for nanothermometry operating over 1000 nm†

Erving C. Ximendes,^{‡a,c} Alexandro F. Pereira,^{‡a} Uéslen Rocha,^a Wagner F. Silva,^a Daniel Jaque^{Ⓜb,c} and Carlos Jacinto^{Ⓜ*a}

The use and applications of infrared emitting rare-earth luminescent nanoparticles as nanothermometers have attracted a great deal of attention during the last few years. Researchers have regarded rare-earth doped luminescent nanoparticles as appealing systems due to their reliability, sensitivity and versatility for minimally invasive thermal sensing in nanomedicine. The challenge of developing nanothermometers operating over 1000 nm with outstanding brightness and enhanced sensitivity is being constantly addressed. In this sense, this work explores the potential of Tm³⁺ emissions at around 1.23 and 1.47 μm, under excitation at 690 nm, for ratiometric thermometry in Tm³⁺ doped LaF₃ nanoparticles. The temperature dependence of the 1.23 μm emission band, which cannot be observed in systems such as NaNbO₃:Tm, was demonstrated to be very effective and presented a relative thermal sensitivity as high as 1.9% °C⁻¹. The physical mechanisms behind the strong thermal dependences were explained in terms of multiphonon decays and cross-relaxations. As a proof of concept, the nanothermometers presented were capable of accessing the basic properties of tissues in an *ex vivo* experiment using thermal relaxation dynamics.

Received 3rd January 2019,
Accepted 4th April 2019

DOI: 10.1039/c9nr00082h
rsc.li/nanoscale

Introduction

Temperature is a fundamental parameter and knowledge of it is essential in industry, electronics, engineering, medicine and many other scientific areas. Among the various existing methods for determining temperature, the use of minimally invasive thermometers stands out as one of the most pursued. As a matter of fact, since contact thermometers (such as thermocouples, pyrometers and thermistors) do not present any suitability for temperature measurements at scales below 10 μm, a new class of thermometers with micrometric and nanometric resolutions needs to be developed. As a particular example of this new class of thermometers, one can mention luminescent nanothermometers (LNThs). The use of LNThs has provided novel methods to understand the thermal behavior of a great variety of micro/nano sized systems and they have received a great deal of attention in the last few years.^{1–10} They

are, in essence, luminescent nanoparticles (LNPs) whose spectral properties (such as emission intensity, spectral shape, lifetime, band peak position, bandwidth, *etc.*) experience significant changes under temperature variations within a specific temperature range [*e.g.*, in the physiological range (36–42 °C)]. The motivation behind the growing interest in the use of LNThs arises not only from a technical point of view (luminescence detection is easy) but also from the promising bio-applications they might have. In fact, LNThs have been already demonstrated to be capable of accessing the basic properties of living tissues and of detecting cardiovascular malfunctions in small animal models among other disfunctions.^{1,9,11–13}

For the past few years, a diverse set of nanomaterials has been used as LNThs. Metallic NPs, quantum dots (QDs), carbon nanotubes, and rare-earth based NPs are just a few of the vast number of examples.^{11,12,14,15} In particular, LNThs based on rare-earth ions (hereafter RE:LNThs) have received great attention due to their intrinsic outstanding optical properties (long fluorescence lifetimes, narrow absorption and emission bands, high photo-stability, and large Stokes shifts).^{16–18} In broad terms, they can be classified into two successful groups: (i) UV/VIS-emitting RE:LNThs under infrared (IR) excitation, *i.e.* NPs which are excited in the IR region but emit outside of it. A good example would be upconversion NPs which convert long wavelength radiation (*e.g.*, IR light) into short wavelength fluorescence (*e.g.*, visible light) *via* a two-

^aGroup of Nano-Photonics and Imaging, Instituto de Física, Universidade Federal de Alagoas, 57072-900 Maceió-AL, Brazil. E-mail: cjacinto@fis.ufal.br

^bFluorescence Imaging Group, Facultad de Ciencias, Universidad Autónoma de Madrid, 28049 Madrid, Spain

^cNanobiology Group, FIRYCIS Hospital Ramon y Cajal, CR. Colmenar, Km 9100, 28034 Madrid, Spain

†Electronic supplementary information (ESI) available. See DOI: 10.1039/c9nr00082h

‡These authors gave equal contributions to the work.

photon or multi-photon mechanism; and (ii) IR–IR RE:LNTs, *i.e.* LNPs excited and emitting within the IR. The second category (IR–IR RE:LNTs), however, presents greater potential for deep tissue diagnosis due to the fact that both excitation and emission bands of most IR–IR RE:LNTs are found within spectral regions, known as biological windows (BWs), where light penetration into biological tissues is maximized and where tissue auto-fluorescence is minimized. As a result, special attention has been paid to their development. Traditionally, three BWs are defined in the literature: I-BW covers the range of 650–950 nm, II-BW covers the range of 1000–1400 nm and III-BW covers the range of 1500–1750 nm.^{19–21} Many different types of RE:LNTs working in these spectral ranges have already been successfully used for fluorescence *in vivo* imaging and photothermal therapy.^{22–24} Despite good results, most of the IR–IR RE:LNTs have the main drawback of low thermal sensitivity. This is the case for Nd/Yb:LaF₃, Nd:NAYF₄, Nd:YAG, and Nd:LaF₃ with reported thermal sensitivities of up to 0.1% °C⁻¹.^{25–30} Thus, the development of highly sensitive IR–IR LNTs remains a subject yet to be thoroughly explored.

In this work, we report a systematic study on the infrared luminescence properties of Tm:LaF₃ NPs and the effect of Tm³⁺ concentration on the ratiometric fluorescence thermal sensing. The overall improvement in thermal sensing caused by tailoring the optimal amount of Tm ions inside the NPs was demonstrated. Also, the potential application of Tm:LaF₃ NPs for high sensitivity nanothermometry in the biological temperature range was analyzed.

Experiments

Synthesis of nanoparticles

The Tm³⁺ doped LaF₃ (Tm³⁺: 1, 3, and 5 mol%) NPs used in this work were prepared by the wet-chemistry method, using lanthanum(III) chloride (LaCl₃, 99.9%), thulium(III) chloride (TmCl₃, 99.9%) and ammonium fluoride (NH₄F, 99.9%) reagents. These were purchased from Sigma-Aldrich to be used directly as reagents, without additional purification. Typically, *X* mol of LaCl₃ (*X* = 0.99, 0.97 and 0.95) and *Y* mol of TmCl₃ (*Y* = 0.01, 0.03 and 0.05) were added to 80 mL of distilled water in a round bottom single neck flask under continuous stirring for 15 min, and heated up to 75 °C. Then, 3 mol of NH₄F was diluted in 3 mL of distilled water and added dropwise to the above mixed chemical solution. The mixture was kept at 75 °C for 3 h at ambient pressure under continuous stirring. A white suspension was formed gradually upon stirring. The nanoparticles obtained were collected by centrifugation at 9000 rpm for 10 min. The precipitate was washed with distilled water several times, centrifuged at 11 000 rpm for 15 min and dried at 60 °C under an ambient atmosphere for 48 h. Finally, the nanoparticles were submitted to heat treatment at 500 °C for 3 h.

Fluorescence thermometry experiments

The fluorescence experiments were performed with Tm³⁺ doped LaF₃ NPs (Tm³⁺ = 1, 3, and 5 mol%) in powder form. The samples were optically excited at 690 nm or 790 nm with a femtosecond Ti:sapphire laser (Coherent, model Chameleon Ultra II) with a repetition rate of 80 MHz, *i.e.*, practically in the continuous wave regime. The generated fluorescence was collected using an optical fiber coupled to a high-resolution spectrometer (a 64 cm single-grated monochromator with 0.1 nm resolution – McPHERSON, model 207), which allows for accurate spectral analysis in the 300–3000 nm spectral range. The luminescence signal was detected using an InGaAs photodiode of 3 mm area with spectral response in the 800–1700 nm range. This detector was coupled to an amplifier lock-in (Stanford Research System, model SR530) and to a computer for signal processing. Temperature induced modifications in the near-infrared (1150 nm–1600 nm) luminescence of the Tm:LaF₃ NPs were investigated by placing the powder inside a homemade temperature controller operating from room temperature up to ~150 °C with an estimated temperature stability close to (or smaller than) 0.5 °C.

Transmission electron microscopy

The particle size and morphology were evaluated using a transmission electron microscope (TEM, TECNAI G2 with a resolution of 0.2 nm) with an accelerating voltage of 200 kV. For TEM investigations, powders were suspended in a water solution, and a drop of this suspension was placed on a holey carbon-coated film supported on a 300 mesh copper grid.

Results and discussion

Tm:LaF₃ as a nanothermometer operating over 1000 nm

The room-temperature normalized photoluminescence spectra in the near-infrared (NIR) region (1100 nm–1575 nm) emanating from the Tm:LaF₃ NPs doped with 1, 3, and 5 mol% of Tm³⁺ (hereafter LaF₃:1Tm, LaF₃:3Tm, and LaF₃:5Tm NPs, respectively), under 690 nm (top) and 790 nm (bottom) excitation (100 mW of pump power) are shown in Fig. 1a. As one can see, the luminescence spectra consisted of two major bands in the NIR with peaks centered at around 1230 nm and 1470 nm. These two bands did not present any overlap and their peaks were well-separated ($\Delta\lambda \sim 230$ nm). They were the result of the ³H₅ → ³H₆ (1230 nm) and ³H₄ → ³F₄ (1470 nm) electronic transitions between characteristic energy levels of Tm³⁺ ions,³¹ as shown in the simplified energy level diagram depicted in Fig. 1b.

Fig. 1a reveals an increment in the relative contribution of the 1230 nm to the overall emission spectra with increasing Tm³⁺ concentration. The overall emission, on the other hand, decreases as a result of concentration quenching (cross-relaxation (CR) between Tm³⁺ ions) and multiphonon decays (Fig. S1 and S3 of the ESI†).³² The mechanism behind this is illustrated in Fig. 1b. The CR2 represented as $\gamma_{CR,2}$ efficiently favors the population of the ³H₅ level. At room temperature,

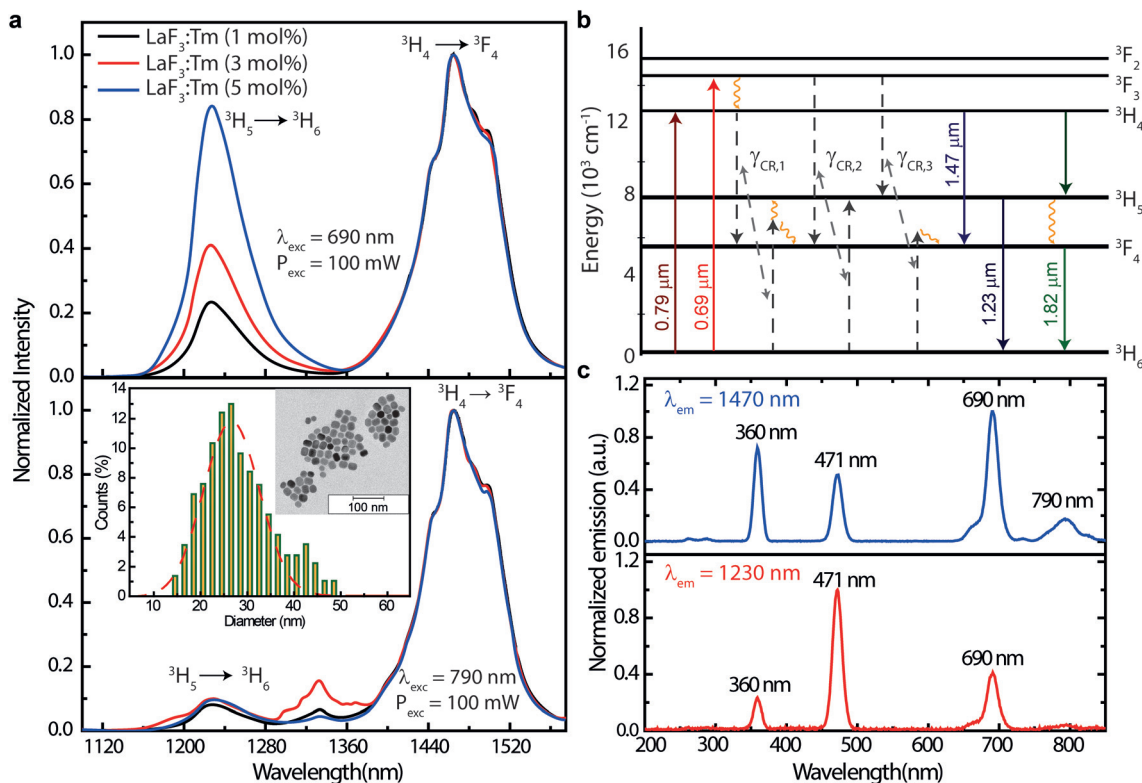


Fig. 1 (a) Normalized emission spectra for the three LaF₃ samples doped with 1, 3, and 5 mol% of Tm³⁺ under excitation at 690 nm (top) and 790 nm (bottom), both with 100 mW of pump power. The inset shows a size histogram as obtained from the statistical analysis of the TEM images corresponding to the LaF₃ sample doped with 5 mol% of Tm³⁺. (b) Simplified energy level diagram for the Tm:LaF₃ system under excitation at 790 or 690 nm. (c) Excitation spectra for the emission at (top) 1470 nm and (bottom) 1230 nm for the 1 mol% Tm doped LaF₃ sample.

the multiphonon decay rate relative to the ${}^3\text{H}_4\text{-}{}^3\text{H}_5$ transition is three orders of magnitude smaller than that of the ${}^3\text{H}_5\text{-}{}^3\text{F}_4$ transition (Fig. S3 of the ESI†). This, in turn, causes the overall emission intensity to decrease with an increase in the number of interacting Tm³⁺ ions. The bottom of Fig. 1a shows a considerably lower fluorescence intensity at 1230 nm than at 1470 nm when using a 790 nm excitation. This, in turn, is explained by the inefficient population of the ${}^3\text{H}_5$ level due to the small branching ratio of the ${}^3\text{H}_4 \rightarrow {}^3\text{H}_5$ transition and the low phonon energy of the LaF₃ host (<400 cm⁻¹)³³ that prevents multiphonon decay in this energy gap. On the other hand, under 690 nm excitation, the relative contribution of the 1230 nm emission increases, reaching a value close to the one at 1470 nm for samples doped with 5 mol% of Tm³⁺. In this case, the ${}^3\text{H}_5$ level is more efficiently populated by means of the CR ${}^3\text{F}_3$, ${}^3\text{H}_6 \rightarrow {}^3\text{F}_4$, ${}^3\text{H}_5$. In fact, this is observed in the higher 1230 nm signal for samples with higher Tm³⁺ concentrations. The necessity and efficiency of using 690 nm as the excitation wavelength is demonstrated from the excitation spectra, as shown in Fig. 1c. Both bands (1230 and 1470 nm) demonstrated to have been much more efficiently excited at 690 nm than at 790 nm. In order to demonstrate the nanometric size of the particles proposed herein, a size histogram obtained from the statistical analysis of TEM images is included as an inset in Fig. 1a. This analysis, in turn, provided

an average size of 25 ± 9 nm for the LaF₃ samples doped with 5 mol% of Tm³⁺. More information on the nanomaterial's characterization, such as XRD and FTIR spectra, can be found in the ESI†

At this point, it is worth noting that even though the recently proposed Tm³⁺ doped NCs of NaNbO₃ constituted a very efficient up-and down-converting system, no emission centered at 1230 nm was observed when utilizing them under the same experimental conditions (Fig. S2 of the ESI†). We believe that the reason for this lies in the high phonon energy of the NaNbO₃ host (around 650 cm⁻¹).³⁴⁻³⁷

Once the emission bands of Tm:LaF₃ NPs were observed under different excitation wavelengths, their potential for luminescent thermometry was investigated. In this sense, their emission spectra, as obtained under 690 nm laser excitation, were analyzed as a function of temperature in the 24–88 °C range. Fig. 2 depicts the normalized emission spectra, for all the investigated samples, as obtained at 24 and 88 °C. As one can see, the overall emission reduces with increasing temperature. The reduction in the emission around 1230 nm, however, is much more emphatic. The effect becomes even more perceptible if one increases the ion concentration. This reduction in the overall emission originates from the thermal dependence of the cross-relaxation energy transfer and from multiphonon relaxation. The clearer reduction of the 1230 nm emission, in

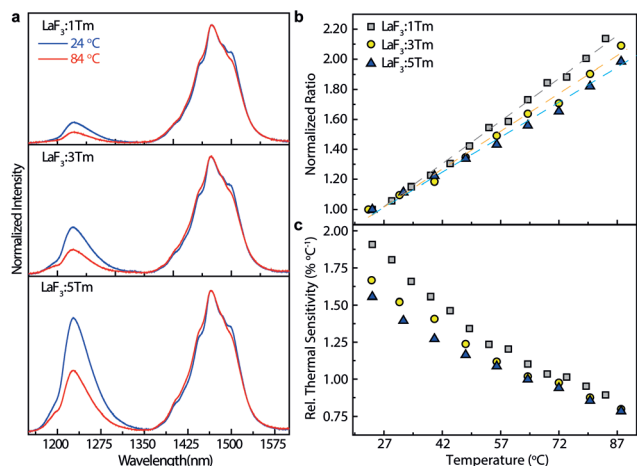


Fig. 2 (a) Normalized emission spectra as obtained at 24 °C (blue) and 84 °C (red) for LaF₃:1Tm, LaF₃:3Tm and LaF₃:5Tm NPs under 690 nm excitation and 100 mW of pump power. (b) Ratio between the emission intensities at 1470 and 1230 nm versus the temperature as normalized by the initial value (corresponding to $T = 24$ °C). (c) Relative thermal sensitivity [$S_r = (1/\Delta)|\partial\Delta/\partial T|$] versus temperature for LaF₃:1Tm, LaF₃:3Tm and LaF₃:5Tm NPs.

turn, takes place due to the fact that the $^3H_5 \rightarrow ^3F_4$ transition presents a larger multiphonon decay rate than the $^3H_4 \rightarrow ^3H_5$ transition (the discussion in Fig. S3 of the ESI† includes a more detailed description about this temperature behavior). Thus, the variations observed in Fig. 2a open the avenue to use the ratio between the emitted intensity of Tm³⁺ ions at 1470 nm ($^3H_4 \rightarrow ^3F_4$, hereafter $I_{1470 \text{ nm}}$) and at 1230 nm ($^3H_5 \rightarrow ^3H_6$, hereafter $I_{1230 \text{ nm}}$). Fig. 2b shows the temperature variation of the intensity ratio $\Delta = I_{1470 \text{ nm}}/I_{1230 \text{ nm}}$ as obtained for all three samples in this work ($I_{1470 \text{ nm}}$ and $I_{1230 \text{ nm}}$ representing the peak intensities). A linear calibration between Δ and T was obtained which, in turn, allowed the estimation of the relative thermal sensitivity $S_r = (1/\Delta)|\partial\Delta/\partial T|$ of all three samples. The results are summarized in Fig. 2c. We have obtained relative thermal sensitivities of 1.90, 1.65 and 1.56% °C⁻¹ for LaF₃:1Tm, LaF₃:3Tm and LaF₃:5Tm NPs, respectively, at 24 °C.

Tm:LaF₃ nanothermometer for analyses *via* thermal relaxation dynamics

Once the thermal sensing capability of Tm:LaF₃ NPs was demonstrated, their potential use for real-time subcutaneous thermometry was also evaluated. As previous studies have stated, when a tissue is undergoing a thermal relaxation process (cooling in the absence of any heating source), the cooling dynamics strongly depends on the basic properties of the tissue.^{11,12,38–40} Thus, accurate measurements of the cooling relaxation profiles provide information about the “tissue status” and, hence, could, in principle, be used to detect anomalies caused by incipient diseases.¹² In this sense, a simple *ex vivo* experiment, aiming to constitute a clear proof of concept, was designed. We injected 0.2 mL of an aqueous

solution of LaF₃:1Tm NPs (10% in mass) into a chicken breast (optical and fluorescence images of this solution are included in Fig. S7 of the ESI†). The injection depth was estimated to be around 1.0 mm. The choice of LaF₃:1Tm NPs over LaF₃:3Tm and LaF₃:5Tm NPs was motivated by the fact that this particular Tm³⁺ concentration presented the higher relative thermal sensitivity (Fig. 2c). A moderate temperature increment at the injection site was induced by producing a hot airflow over the surface of the tissue (Fig. 3a). In this experiment, a cw fiber coupled diode laser was used as the excitation source operating at 690 nm. At this moment, it is important to point out that the emission spectra do not present any difference to those obtained using the chameleon laser as an excitation source. Optical excitation and subsequent luminescence collection were both performed by using a single long working distance objective. Spectral analysis of the subcutaneous NP fluorescence was used to estimate the injection’s temperature by evaluating Δ . Data included in Fig. 3b present the thermal relaxation dynamics as obtained after following these procedures.

As previous studies have stated, the subcutaneous thermal relaxation of the tissue with a negligible perfusion rate is well described by:

$$T_{\text{scut}} = T_{\infty} + \Delta T_{\text{scut}} \text{erf}\left(\sqrt{\tau/t}\right) \quad (1)$$

where erf denotes the Gaussian error function, τ is the characteristic tissue relaxation time and ΔT_{scut} is the temperature difference between the initial temperature and T_{∞} . We note that τ is determined by the tissue’s thermal properties, so that it is given by:^{38,41}

$$\tau = L^2/4\alpha_{\text{tissue}} \quad (2)$$

in which L is a parameter known as the characteristic length of the tissue and α_{tissue} is its thermal diffusivity.

After fitting the data in Fig. 3b to eqn (1) (red solid line), we obtained the values of 27 °C, 11 °C and 22 s for T_{∞} , ΔT_{scut} and τ , respectively. In previous studies, we have explored the possibility of evaluating the tissue thermal diffusivity by means of eqn (2).¹¹ There, we had set L , the characteristic length/dimen-

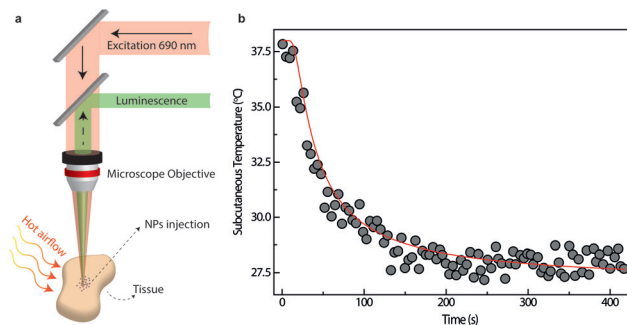


Fig. 3 (a) Experimental setup of the thermal relaxation dynamics experiment in the *ex vivo* tissue. (b) Thermal relaxation of the *ex vivo* tissue as obtained *via* optical thermometry based on Tm:LaF₃ NPs.

sion of the tissue undergoing the thermal relaxation, as equal to the penetration depth of the laser radiation inducing the surface temperature increment. In the experiment depicted in Fig. 3a, however, we have a hot airflow as the main factor responsible for surface temperature increment. Determining the penetration depth of the heat being transported under these experimental conditions, in turn, is not an easy task. Thus, instead of using L to determine α , we will use τ in order to determine L . By using published data for thermal conductivity ($k_{\text{tissue}} = 0.488 \text{ W m}^{-1} \text{ }^{\circ}\text{C}^{-1}$), density ($\rho_{\text{tissue}} = 10^3 \text{ kg m}^{-3}$) and specific heat ($c_{\text{tissue}} = 3.3 \times 10^3 \text{ J kg}^{-1} \text{ }^{\circ}\text{C}^{-1}$) of chicken breast tissues, one obtains $\alpha_{\text{tissue}} = k_{\text{tissue}}/\rho_{\text{tissue}}c_{\text{tissue}} = 0.147 \text{ mm}^2 \text{ s}^{-1}$.^{42–44} Therefore, $L = \sqrt{4\tau\alpha_{\text{tissue}}} \approx 3.60 \text{ nm}$. Data included in Fig. 3 demonstrate that our LaF₃:1Tm NPs are capable of accessing the basic parameters describing heat transfer in biological tissues by means of time resolved thermal reading over a subcutaneous thermal relaxation.

Conclusions

The potential application of Tm³⁺ doped lanthanum fluoride nanoparticles (Tm:LaF₃) with different doping concentrations was thoroughly investigated in this work. The NP luminescence spectra consisted of two major bands in the NIR, with peaks centered at around 1230 nm and 1470 nm. It has been shown that both bands were much more efficiently excited at 690 nm and that a significant thermally dependent reduction in the emission around 1230 nm took place due to a larger multiphonon decay presented by the ³H₅ → ³F₄ transition. As a consequence, the thermal sensing capability of Tm:LaF₃ NPs was demonstrated as they achieved relative thermal sensitivities as high as 1.9% °C⁻¹ in the physiological temperature range. Furthermore, since both emission bands were found within the NIR, their potential use for real-time subcutaneous thermometry was also evaluated. It was demonstrated that Tm:LaF₃ NPs were capable of accessing the basic properties of heat dissipation inside an *ex vivo* tissue. Thus, the results reported here demonstrate the bright potential of NIR emitting nanothermometers in the study of heat transfer inside biological tissues.

Conflicts of interest

There are no conflicts to declare.

Acknowledgements

This work was carried out under the support of Brazilian Agencies: FINEP (Financiadora de Estudos e Projetos) through the grants INFRAPESQ-11 and INFRAPESQ-12; CNPq (Conselho Nacional de Desenvolvimento Científico e Tecnológico) grant INCT NANO(BIO) SIMES and Project Universal no. 431736/2018-9; CAPES (Coordenadoria de Aperfeiçoamento de Pessoal de Ensino Superior) by means of

the Project PVE no. A077/2013. E. C. X. was supported by a PhD scholarship from CNPq and by the PVE A077/2013 project by means of a PhD sandwich program developed at the Universidad Autonoma de Madrid, Spain. D. J. is the PVE (Pesquisador Visitante Especial) of the Project A077/2013. A. F. P was supported by a PhD scholarship from CNPq. This work has also been funded by Ministerio de Economía y Competitividad-MINECO (MAT2016-75362-C3-1-R) and the Comunidad de Madrid (B2017/BMD-3867 RENIM-CM) co-financed by European Structural and Investment Fund.

References

- 1 B. del Rosal, E. Ximendes, U. Rocha and D. Jaque, *Adv. Opt. Mater.*, 2017, **5**, 1600508.
- 2 D. Jaque and F. Vetrone, *Nanoscale*, 2012, **4**, 4301.
- 3 X.-Q. Zhang, R. Lam, X. Xu, E. K. Chow, H.-J. Kim and D. Ho, *Adv. Mater.*, 2011, **23**, 4770–4775.
- 4 S. Jiang, M. K. Gnanasammandhan and Y. Zhang, *J. R. Soc., Interface*, 2010, **7**, 3–18.
- 5 E. Boisselier and D. Astruc, *Chem. Soc. Rev.*, 2009, **38**, 1759.
- 6 I. Brigger, C. Dubernet and P. Couvreur, *Adv. Drug Delivery Rev.*, 2002, **54**, 631–651.
- 7 L. Labrador-Páez, E. C. Ximendes, P. Rodríguez-Sevilla, D. H. Ortgies, U. Rocha, C. Jacinto, E. Martín Rodríguez, P. Haro-González and D. Jaque, *Nanoscale*, 2018, **10**, 12935.
- 8 A. F. Pereira, J. F. Silva, A. S. Gouveia-Neto and C. Jacinto, *Sens. Actuators, B*, 2017, **238**, 525–531.
- 9 M. Xu, X. Zou, Q. Su, W. Yuan, C. Cao, Q. Wang, X. Zhu, W. Feng and F. Li, *Nat. Commun.*, 2018, **9**, 2698.
- 10 S. Sekiyama, M. Umezawa, S. Kuraoka, T. Ube, M. Kamimura and K. Soga, *Sci. Rep.*, 2018, **8**, 16979.
- 11 E. C. Ximendes, W. Q. Santos, U. Rocha, U. K. Kagola, F. Sanz-Rodríguez, N. Fernandez, A. da S. Gouveia-Neto, D. Bravo, A. M. Domingo, B. del Rosal, C. D. S. Brites, L. D. Carlos, D. Jaque and C. Jacinto, *Nano Lett.*, 2016, **16**, 1695–1703.
- 12 E. C. Ximendes, U. Rocha, B. del Rosal, A. Vaquero, F. Sanz-Rodríguez, L. Monge, F. Ren, F. Vetrone, D. Ma, J. García-Solé, C. Jacinto, D. Jaque and N. Fernández, *Adv. Healthcare Mater.*, 2017, **6**, 1601195.
- 13 D. Jaque, C. Richard, B. Viana, K. Soga, X. Liu and J. García Solé, *Adv. Opt. Photonics*, 2016, **8**, 1.
- 14 X. Zhu, W. Feng, J. Chang, Y.-W. Tan, J. Li, M. Chen, Y. Sun and F. Li, *Nat. Commun.*, 2016, **7**, 10437.
- 15 B. del Rosal, E. Carrasco, F. Ren, A. Benayas, F. Vetrone, F. Sanz-Rodríguez, D. Ma, Á. Juarranz and D. Jaque, *Adv. Funct. Mater.*, 2016, **26**, 6060–6068.
- 16 M. Quintanilla, A. Benayas, R. Naccache and F. Vetrone, in *Nanoscience & Nanotechnology Series*, ed. L. D. Carlos and F. Palacio, Royal Society of Chemistry, Cambridge, 2015, pp. 124–166.
- 17 C. D. S. Brites, P. P. Lima, N. J. O. Silva, A. Millán, V. S. Amaral, F. Palacio and L. D. Carlos, *J. Lumin.*, 2013, **133**, 230–232.

- 18 C. D. S. Brites, A. Millán and L. D. Carlos, in *Handbook on the Physics and Chemistry of Rare Earths*, Elsevier, 2016, vol. 49, pp. 339–427.
- 19 J. Xu, D. Murata, J. Ueda and S. Tanabe, *J. Mater. Chem. C*, 2016, **4**, 11096–11103.
- 20 E. Hemmer, N. Venkatachalam, H. Hyodo, A. Hattori, Y. Ebina, H. Kishimoto and K. Soga, *Nanoscale*, 2013, **5**, 11339.
- 21 A. M. Smith, M. C. Mancini and S. Nie, *Nat. Nanotechnol.*, 2009, **4**, 710–711.
- 22 J. Zhou, Y. Sun, X. Du, L. Xiong, H. Hu and F. Li, *Biomaterials*, 2010, **31**, 3287–3295.
- 23 D. J. Naczynski, M. C. Tan, M. Zevon, B. Wall, J. Kohl, A. Kulesa, S. Chen, C. M. Roth, R. E. Riman and P. V. Moghe, *Nat. Commun.*, 2013, **4**, 2199.
- 24 Y. Zhong, Z. Ma, S. Zhu, J. Yue, M. Zhang, A. L. Antaris, J. Yuan, R. Cui, H. Wan, Y. Zhou, W. Wang, N. F. Huang, J. Luo, Z. Hu and H. Dai, *Nat. Commun.*, 2017, **8**, 737.
- 25 C. Wang, L. Xu, J. Xu, D. Yang, B. Liu, S. Gai, F. He and P. Yang, *Dalton Trans.*, 2017, **46**, 12147–12157.
- 26 R. Lv, C. Zhong, R. Li, P. Yang, F. He, S. Gai, Z. Hou, G. Yang and J. Lin, *Chem. Mater.*, 2015, **27**, 1751–1763.
- 27 T. Shen, Y. Zhang, A. M. Kirillov, B. Hu, C. Shan, W. Liu and Y. Tang, *J. Mater. Chem. B*, 2016, **4**, 7832–7844.
- 28 U. Rocha, C. Jacinto, W. F. Silva, I. Guedes, A. Benayas, L. M. Maestro, M. Acosta Elias, E. Bovero, F. C. J. M. van Veggel, J. García-Solé and D. Jaque, *ACS Nano*, 2013, **7**, 1188–1199.
- 29 U. Rocha, C. Jacinto, K. U. Kumar, F. J. López, D. Bravo, J. G. Solé and D. Jaque, *J. Lumin.*, 2016, **175**, 149–157.
- 30 A. Benayas, B. del Rosal, A. Pérez-Delgado, K. Santacruz-Gómez, D. Jaque, G. A. Hirata and F. Vetrone, *Adv. Opt. Mater.*, 2015, **3**, 687–694.
- 31 X. Bai, D. Li, Q. Liu, B. Dong, S. Xu and H. Song, *J. Mater. Chem.*, 2012, **22**, 24698.
- 32 J. F. Suyver, J. Grimm, M. K. van Veen, D. Biner, K. W. Krämer and H. U. Güdel, *J. Lumin.*, 2006, **117**, 1–12.
- 33 Z. Xiaoting, T. Hayakawa, Y. Ishikawa, Y. Liushuan and M. Nogami, *J. Alloys Compd.*, 2015, **644**, 77–81.
- 34 K. U. Kumar, K. Linganna, S. S. Babu, F. Piccinelli, A. Speghini, M. Giarola, G. Mariotto and C. K. Jayasankar, *Sci. Adv. Mater.*, 2012, **4**, 584–590.
- 35 A. F. Pereira, K. U. Kumar, W. F. Silva, W. Q. Santos, D. Jaque and C. Jacinto, *Sens. Actuators, B*, 2015, **213**, 65–71.
- 36 K. U. Kumar, W. Q. Santos, W. F. Silva and C. Jacinto, *J. Nanosci. Nanotechnol.*, 2013, **13**, 6841–6845.
- 37 K. U. Kumar, W. F. Silva, K. Venkata Krishnaiah, C. K. Jayasankar and C. Jacinto, *J. Nanophotonics*, 2014, **8**, 083093.
- 38 N. Furzikov, *IEEE J. Quantum Electron.*, 1987, **23**, 1751–1755.
- 39 E. C. Ximendes, U. Rocha, T. O. Sales, N. Fernández, F. Sanz-Rodríguez, I. R. Martín, C. Jacinto and D. Jaque, *Adv. Funct. Mater.*, 2017, **27**, 1702249.
- 40 H. D. A. Santos, E. C. Ximendes, M. del C. Iglesias-de la Cruz, I. Chaves-Coira, B. del Rosal, C. Jacinto, L. Monge, I. Rubia-Rodríguez, D. Ortega, S. Mateos, J. GarcíaSolé, D. Jaque and N. Fernández, *Adv. Funct. Mater.*, 2018, **28**, 1803924.
- 41 J. W. Valvano, in *Optical-Thermal Response of Laser-Irradiated Tissue*, ed. A. J. Welch and M. J. C. van Gemert, Springer Netherlands, Dordrecht, 2010, pp. 455–485.
- 42 V. E. Sweat, C. G. Haugh and W. J. Stadelman, *J. Food Sci.*, 1973, **38**, 158–160.
- 43 R. Y. Murphy, B. P. Marks and J. A. Marcy, *J. Food Sci.*, 1998, **63**, 88–91.
- 44 K. Giering, I. Lamprecht, O. Minet and A. Handke, *Thermochim. Acta*, 1995, **251**, 199–205.